New Coupling Agent Structures for Preparing Filler-Polymer Hybrid Materials Under Soft Irradiation Conditions

Houssein Nasrallah, Rita Zakhia Douaihy, Igor Telegeiev, Oleg I Lebedev, Armand Fahs, Mohamad El-Roz

New coupling agent structures for preparing filler-polymer hybrid materials under soft-irradiation conditions

*Houssein Nasrallah[a]‡, Rita Zakhia Douaihy[a]‡, Igor Telegeiev [a], Oleg I. Lebedev [b], Armand Fahs[c], Mohamad EL-Roz[a]**

[a]Normandie Université, ENSICAEN, UNICAEN, CNRS, Laboratoire Catalyse et Spectrochimie, 14050 Caen, France.

[b]Normandie Université, ENSICAEN, UNICAEN, CNRS, Laboratoire CRISMAT, 14050 Caen, France.

[c] Université de Toulon, Laboratoire MAPIEM, 83041 Toulon, France

KEYWORDS: Silane Based Photoinitiator (SPI), hybrid materials, silica, polymer, photolithography

ABSTRACT: The bifunctional coupling agents have become unavoidable products for preparing hybrid materials with enhanced properties. They are at the origin of the homogeneous dispersion of the filler in the polymerizable matrix and the strong chemical interactions between the composites during the thermal reticulation and vulcanization processes. However, only few structures can play this role in a photo-curable matrix, which is widely applied today in various

manufactures (3D printing, cosmetic, medicine, etc.). Developing new structures capable of working under accurate irradiation conditions can extend the use of coupling agents for preparing hybrid photo-curable materials for various applications (e.g. membrane, masks, 2D- and 3D-nano/micro-objects). Recently, a new SPI (**SPI-1**) was proposed by our group and has revealed a high efficiency for preparing filler-polymer hybrid material. Despite its efficiency, its activity is the highest under the UV-B irradiation but lower under UV-A and inactive under visible light. In this paper, new coupling agent structures (bifunctional Silane-based Photoinitiators; SPI) are synthesized and tested under various irradiation conditions extensively used in the photocuring fields (365, 385 and 405 nm). All the new structures demonstrate higher performance than the first SPI generation (**SPI-1**) under the diverse light sources. More particularly, SPI-**4**, **5**, and **6** (triphenylamine-based SPI) demonstrate a remarkable activity for preparing filler-polymer hybrid materials under visible light irradiation (LED 405 nm). The efficiency of the new structures in the photopolymerization as well as in the grafting of the silica particles (used as filler model) is elucidated. Finally, the enhancement of the mechanical properties of the hybrid composite films and the possible use of the new approach in photolithography is also demonstrated.

1. **INTRODUCTION**

Coupling agents have been widely used in the vulcanization processes[1] and thermal polymerization[2, 3]. Their importance has risen from the dual types of their functional groups: one interacts with the organic matrix and one is attached to the surface of the inorganic filler[4, 5]. They enhance the interactions between the inorganic fillers and the polymer matrix by preventing the agglomeration and the formation of clusters and assuring a homogeneous dispersion[6]. Additionally, they improve the interfacial adhesion and therefore the stability and the mechanical

behavior of the formed hybrid materials with respect to the fillers-free polymer[7, 8]. Lately, light induced polymerization has been extensively developed since it can occur under mild conditions, in the absence of organic solvent and at room temperature with excellent spatial and temporal control[9-11]. Photocuring materials have consequently gained great interest since they can be used in the daily consuming[12], electriconics[13] and biomedical products[14-16]. Inspired foremost by the role of the coupling agents, the development of new photoactive and bifunctional coupling agents for the photopolymerization is therefore highly required.

In this context, several coupling agents were developed to enhance the properties of the photocuring materials under UV irradiation such as titanate[17, 18] and silane[19-22]. Among them, a new bifunctional silane-based photoinitiator coupling agent (SPI-1) has been developed recently by our group[23, 24] which ensures strong covalent and chemical interactions between the filler particles and the polymer matrix[25, 26]. Upon UV irradiation, ketyl radicals are engendered on the surface, initiating the polymerization of the acrylate monomer. Thus a homogeneous external polymer layer is obtained on the surface of the silica nanoparticles, creating therefore a hybrid material with enhanced mechanical properties.[24] However, **SPI-1** demonstrates activity only under UV-B irradiation and is inactive under visible light. If the synthesis of photocuring materials under UV light irradiation achieved great interest, some safety concerns have risen from its use including eye and skin damages in addition to associated consumption and energy cost[27, 28]. Thus, 3D-printing systems are modified and adapted to work under near-UV-A (>350 nm) and visible-light irradiations (>390 nm).

To the best of our knowledge, only one photoactive coupling structure with dual activity, inspired from our previous work[23,24], has been very recently synthesized and studied for

photopolymerization under visible light irradiation[29], where a commercial triazine photoinitiator has been silylated, in order to attach the silane functional groups.

Based on the market needs to develop photoinitiator coupling agents active in the visible region and based the promising advantages of the previously synthesized silane based photoinitiator, we aim in this work to widen the efficiency range of the previously synthesized SPI so it can be active under different visible irradiations, considering the cost effective of the proposed structure. The approach consists on the substitution of phenyl group of **SPI-1** by near-UV/Visible responsive aryls while conserving the same linear alkyl-silane group. Thus, thioanisole, pyrene and mono-, di- and tri- substituted triphenylamine based photoinitiators **SPI-2**, -**3**, -**4**, -**5** and -**6** were synthetized, respectively. The efficiency of the new SPI structures is tested in the polymerization of trimethylolpropane triacrylate (TMPTA) under different light sources mostly used in the photocuring technology and commercial public equipment (as 3D-printers): LED 365 nm, LED 385 nm and LED 405 nm. The behaviors of the excited states of the synthesized SPIs are investigated by time-resolved absorption transient spectroscopy. Later, the efficiency of a selected SPI (**SPI-4**) and grafted on the surface of silica nanoparticles, is characterized and tested in the polymerization of TMPTA, and compared to that of the grafted **SPI-1**. Finally, dispersed **SPI-4** in TMPTA is tested in photolithography using an ink-jet printed mask on transparent film in order to test the spatial resolution of the process and study the mechanical properties of the composites.

2. RESULTS AND DISCUSSION

2.1 SPI-X synthesis and characterization

The synthesis of **SPI-1** was reported in our previous work starting from isobutyrophenone (**Scheme 1**)[24]. Inspired from this successful and relatively cost-effective approach, a series of new

structures (called **SPI-X**; with **X =2, 3, 4, 5** and **6**) was prepared in the same general synthetic pathway with an additional electrophilic aromatic substitution (EAS) of aryl groups with the isobutyryl group using $AlCl_3$. The SPI's precursors (**P-SPI-X**) were then obtained via a subsequent treatment with allyl bromide in a basic medium to introduce the allylic group. To obtain the new structures, triethoxysilane anchoring group was added to the precursors (**P-SPI-X)** by a platinum catalyzed anti-Markovnikov hydrosilylation using 5 wt.% of Pt on Al_2O_3 catalyst. In the first step (**step 1** in **Scheme 1**), the compounds **P-1-SPI -2** and -**3** were isolated starting from thioanisole and pyrene with yields of 99% and 77 %, respectively. However, to prepare **P-1-SPI -4, -5** and -**6**, a controlled mono-, di-, and tri-electrophilic aromatic substitution of triphenylamine was realized by adjusting the quantity of the isobutyryl chloride **(IBC)** and that of the $AlCl_3$ as well as the temperature of the reaction. This optimization allowed isolating **P-1-SPI -4, -5** and -**6** with 61, 66, and 63% yields, respectively. Subsequently the allylation (**step 2**) was realized by introducing 3 equivalents of allyl bromide for each isobutyryl group to obtain the **P-SPI -2, -3, -4, -5** and **-6** precursors with satisfactory yields (62-80%). Finally, for the hydrosilylation (**step 3**), two equivalents of $HSi(OEt)_3$ were introduced for each allyl group to obtain the **SPI -2, -3, -4, -5** and -**6** structures with yields of 31, 26, 21, 11 and 18 %, and overall yield of 24, 13, 10, 5 and 7%, respectively. The relatively low overall yields are originated essentially from the hydrosilylation step where unidentified by-products with ratio of 50% are obtained. This selectivity issue is due to the heating requirement at 83°C with heterogenous Pt/Al_2O_3 catalyst during the hydrosilylation to achieve higher conversion. Nevertheless, the heterogenous Pt/Al_2O_3 was able to be recycled by filtration and was successfully tested for 3 efficient to obtain **SPI-1** in 60 g scale. On the other hand, the yield of **SPI -4**, **SPI -5,** and **SPI -6** can be significantly enhanced if their corresponding precursors are not separated where mixtures of **SPI-4/SPI-5** and **SPI-5/SPI-6** will be obtained,

respectively. The mixtures will not affect their roles as coupling agents for real applications. However, in this study, the separation was required in order to investigate separately the properties of each structure. The purity of all SPI was always higher than 90% except for **SPI-6** (estimated purity of 70%) due to the difficult separation step from the unidentified by-product. The low overall yield of SPI -4, -5 and -6 can be enhanced by using homogeneous catalyst (e.g. $[IrCODCl]_2$ [30], Ru-based catalyst[31]) in the anti-Markonikov hydrosilylation limiting step and minimizing therefore the by-product due to the use of Pt/Al_2O_3 catalyst at 80°C. However, these catalysts are highly sensitive toward oxygen and moisture and their manipulation should be conducted in inert conditions making the process less costly despite the higher overall yield. In addition, contrary to the heterogeneous Pt/Al_2O_3 which it was recycled and can be used at least for three cycles, the homogeneous catalyst cannot be recycled increasing furthermore the cost of the process. Detailed synthesis procedures, synthesis conditions and NMR spectra of the new structures are given in the supplementary information SI (**Figure S1-Figure S27**).

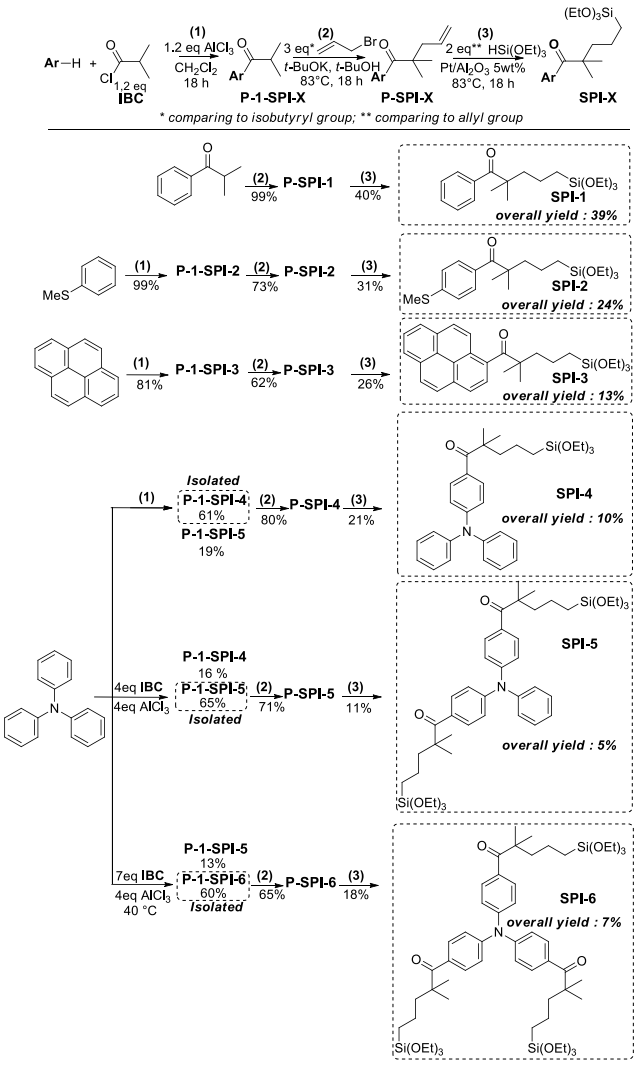

Scheme 1. Illustration of the synthesis approaches of the various SPI structures studied in this work.

After successfully synthesizing the different SPI structures, they were characterized using UV-Visible spectroscopy to determine their optical and electrochemical properties. The molar extinction coefficient for every structure is determined using the Beer-Lambert law **(Figure 1)**. The characteristic band attributed to the electronic transition of the $\pi - \pi^*$ of the benzoyl group is observed in all the UV-Vis spectra of the different SPI structures, in the region between 225 and 300 nm[24]. Additionally, the characteristic band of the electronic transition of the $n - \pi^*$ of the

benzoyl group is observed for **SPI-1** and **SPI-2** at 300 nm. Particularly, for **SPI-2**, the characteristic band of the thioanisole group ($\pi - \pi^*$) at 250 nm is observed [32]. The electronic transitions of the pyrene structure of the **SPI-3** are observed in the region between 250 and 380 nm[33], whereas the electronic transition of $n - \pi^*$ in of the **SPI -4, -5** and **-6** structures are detected between 300 and 400 nm.[34] As investigated, all new structures illustrate a significant redshift in respect to the previous **SPI-1** structures. More particularly, **SPI -4 to -6** demonstrate a promising overlap of their absorbance with the light emission of the various LED irradiations (**Figure 1**) frequently used in the lithography and the 3D-photoresine's printers. It should be noted that **SPI and P-SPI** structures show similar light absorbance profile and therefore siloxane group has no impact on the photochemical behaviors of the SPI.

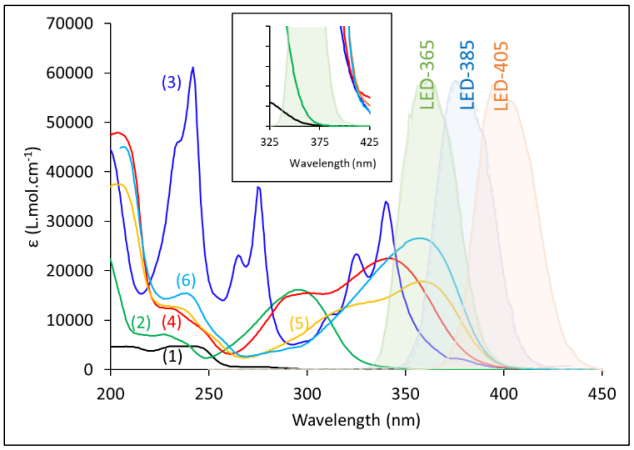

Figure 1. UV-Visible spectra of different SPI structures and spectrum of the different LED lights at different wavelengths. Inset: zooming on the absorbance in the region between 325 and 425 nm.

2.2 Photopolymerization efficiency of the new structures

The activity of the SPI structures (**1**-**6**) in the radical photopolymerization of TMPTA using three different light sources (LED 365 nm, 385 nm and 405 nm) is examined by real time IR

spectroscopy analysis (**Scheme S1**). Due to the relatively low purity of **SPI-6**, the **P-SPI-6** is used after confirming that the precursor and its corresponding structure have similar photopolymerization performances by comparing **SPI-4** with **P-SPI-4** under monochromatic irradiation (365 nm) (**Figure S28**). The kinetics of photopolymerization process was determined by monitoring the evolution of the C=C vibration band (at 1635 cm^{-1}) of the TMPTA monomer using IR spectroscopy and the results are assembled in **Figure 2 (A-F)**. The apparent photopolymerization rate (Rp) and the conversion yields are summarized in **Table S2**.

Under the various irradiation sources, **SPI-1** showed the lowest performance compared to the new SPI structures, with a maximum conversion of 36 % under 365 nm. An induction time (around 20 seconds) is observed for **SPI-2** and **SPI-3** under 365 nm, with a relatively higher conversion for **SPI-3** (39% vs 51%, respectively). The induction time might be explained by the insufficient quantity of the radicals compared to the quantity of the quenchers (e.g. dissolved oxygen, etc.) in the first few seconds of the reaction. The efficiency and the conversion yields of **SPI -2** and **-3** are dramatically affected under 385 nm and 405 nm. However, **SPI-4** shows the highest activity under the various irradiation condition as a mono-silane functionalized structure. These results are in good agreement with the absorbance of the **SPI-4** structure.

The activity of the mono-, di- and tri- substituted triphenylamine based SPI is compared under the same previous conditions (**Figure 2, D-F**). All of them showed good efficiency with TMPTA conversions higher than 30 % with the highest conversion yield for **SPI-6** (**P-SPI-6**). Nevertheless, only **SPI-4** will be considered in our study due the synthesis issue encountered in the preparation of **SPI-5** and -**6** (lower yield and purity, respectively).

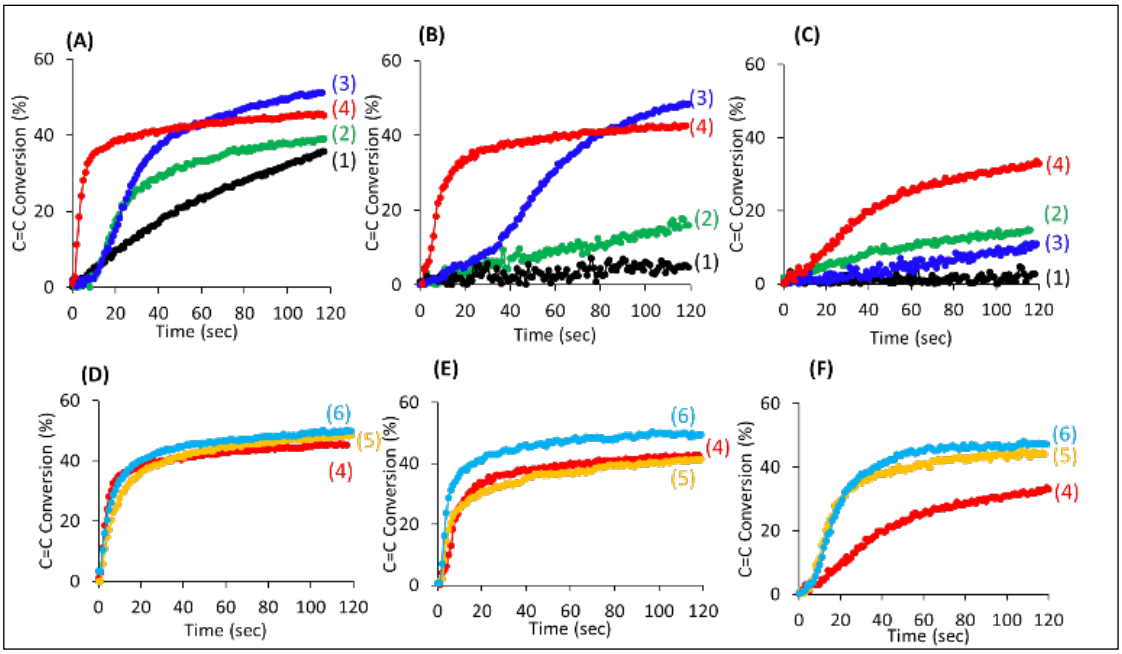

Figure 2. Photopolymerization kinetics of trimethylolpropane triacrylate (TMPTA) under (A) 365 nm, (B) 385 nm and (C) 405 nm of irradiation using 1 wt.% of **SPI-X** as photoinitiators. (D-E) represent the effect of the bi- (**SPI-5**) and tri- (**SPI-6**) siloxane substitution in respect to the monosubstituted structure (**SPI-4**) for photopolymerizing TMPTA under (D) 365 nm, € 385 nm and (F) 405 nm. Photopolymerization performed in laminated (50 μm) condition (air-free); Irradiance = 306.4, 233.7, and 190 mW/cm^2 for LED 365 nm, LED 385 nm and LED 405 nm, respectively.

2.3 Absorption transient of the SPI-X excited states

The time resolved absorption transient spectroscopy shed more light on the behavior of the excited state of the different SPI structures (**Figure 3**). **SPI-1** demonstrates an absorption transient (AT) band centered at 650 nm which corresponds to the absorption of the triplet state of the **SPI-1**. The **SPI -2**'s and **-3**'s AT-spectra reveal two maxima each at 640, 530 nm and at 460, 430 nm, respectively, revealing an impact of the substation group on the photochemical behavior of the excited state. The AT spectra of the **SPI -4**, **-5** and **-6** show low red-shift in respect to **SPI-1,** with

a significant red-shifted bleaching at 340, 350 and 355 nm, respectively. In addition, a residual absorbance with relatively long lifetime could be observed in the visible range (except for **SPI-3**) and probably corresponds to the absorption of the relatively stable benzoyl radicals. It should be noted that the bleaching of **SPI -4**, **-5** and **6** follows an increasing order and confirms the increase of the relative quantum yield with the structure substitution of the triphenylamine.

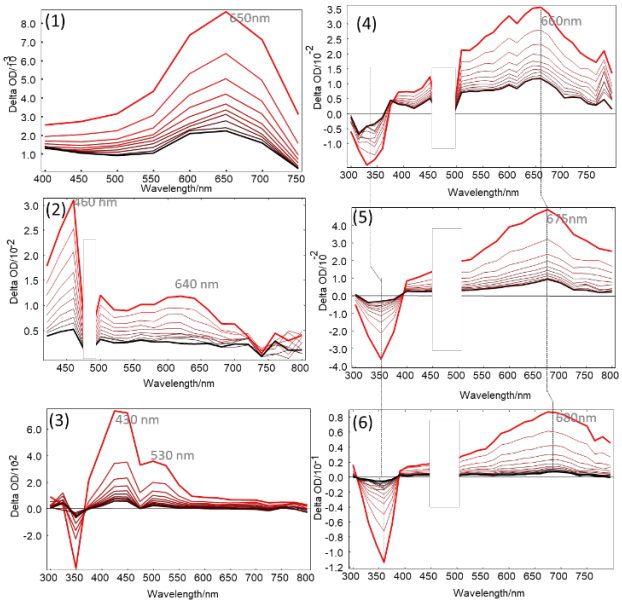

Figure 3. Evolution vs the time (1 μs/spectrum) of the absorption transition (AT) of **SPI-1** (1), **SPI-2** (2), **SPI-3** (3) **SPI-4** (4), **SPI-5** (5) and **SPI-6** (6). All spectra were recorded with an excitation at 355 nm (except **SPI-1** at 266 nm) and resolution of 20 nm. Laser energy 5 to 7 mJ. The optical density of the solution at the excited wavelength was adjusted at around 0.5 a.u. The white zone corresponds to the fluorescence saturation region of the corresponding structures.

Figure 4 (and **Table S3**) assemble the decay (and the absolute lifetime) of the excited state versus time at the corresponding maximum of the absorption transient for each structure (**Figure 3**). The results show a fast quenching of **SPI-3** with respect to the other SPI without any residual absorbance. This could be the main reason of the relatively low activity of this structure. However,

SPI-1 demonstrates similar kinetic decay of the excited state in comparison with **SPI -2**, **-4**, **-5** and **-6**. Therefore, the highest activity is mainly related to their highest absorbance. Nevertheless, it is complicated to reveal with precision the origin of the activity of the new structures as many factors can contribute to the global activity (quantum yield of the different process and activity of the generated radicals). In addition, all structures show high sensitivity toward oxygen with a constant rate of oxygen quenching 3 to 7 10^9 $M^{-1}s^{-1}$ (**Table S3**), which require an oxygen-free photopolymerization process. It is important to mention that the new structures are well designed in a way that the allyl radicals are always attached to the grafted surface, ensuring then an efficient initiation of the polymerization process, and therefore the efficiency of the shell formation around the particle is not altered by the stability of the chromophore/benzoyl radical moiety (due to the increase of the rearrangement with the conjugated bond). This justifies our initial choice to avoid the grafting of the siloxane grafting function on the benzoyl moiety of the SPI structures.

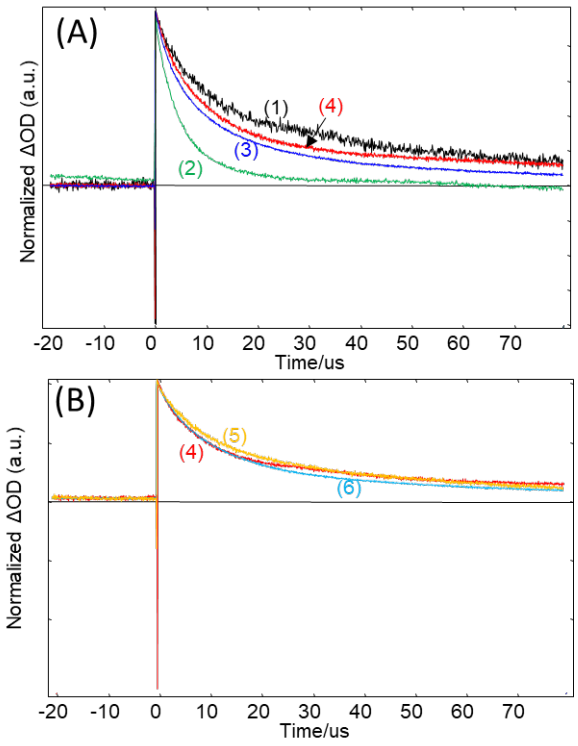

Figure 4. (A) Normalized kinetic decay traces of the triplet excited state of **SPI-1** (1), **SPI-2** (2), **SPI-3** (3) and **SPI-4** (4). (B) Normalized kinetic decay traces of the triplet excited state of **SPI-4** (4), **SPI-5** (5), and **SPI-6** (6). The spectra were registered at the λ max of the absorption transient of the different SPI-structures (Figure 3). The negative region due to the photoluminescence of the products.

2.4 Grafting of SPI-1 and SPI-4 on silica nanoparticles

Based on the previous results, only **SPI-4 and SPI-1** (used as reference) are considered for studying their efficiency in the grafting process of silica nanoparticles (used as filler) and the efficiency of the grafted filler for preparing silica polymer hybrid materials. The grafted silica samples with **SPI-1** and **SPI-4** are firstly characterized using thermogravimetric analysis (**Figure 5(A)**) to quantify the amount of the grafted SPI. A higher weight loss of the grafted silica in comparison to the parent silica (ref) is reported. The evaporation of adsorbed water on the surface of silica particles cause a weight loss at temperatures below 200 °C in all cases. The weight loss below 300 °C for the grafted silica nanoparticles is attributed to the degradation of SPI structure. The weight loss from 300 to 700°C can be accredited to the thermal decomposition and the total oxidation of chemical-bonded groups on the surfaces, as well as to the condensation process of the vicinal silanol groups (the silica dehydration from this process is estimated to be less then 1 wt.% as observed on the pure silica (ref)). Thereby, the results indicate that both **SPI-1** and **SPI-4** are chemically bonded to the silica surface with a loading of 2.55 ±0.05 and 3.1 ±0.05 wt.%, respectively. The higher amount of grafted **SPI-4** is mainly assigned to the higher molar mass of this later with respect to the **SPI-1**.

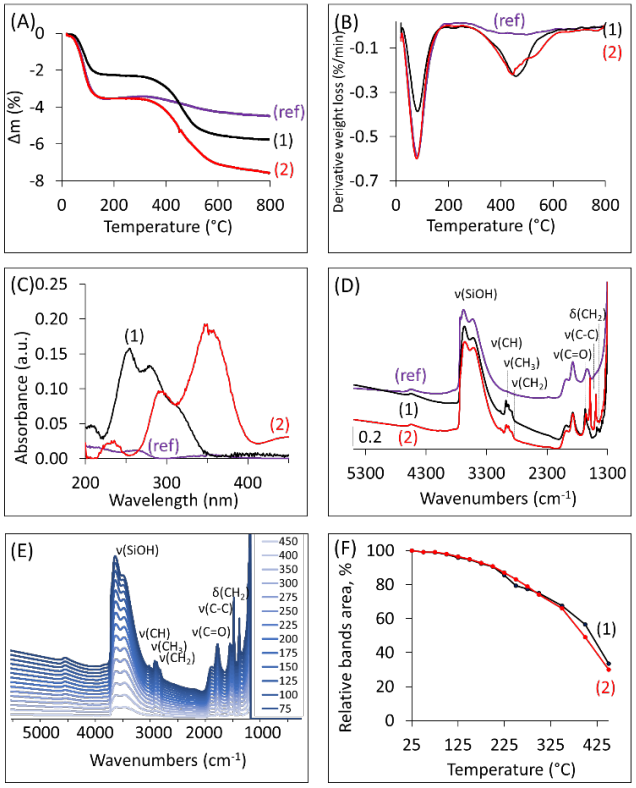

Figure 5. (A) TG, (B) dTG, (C), UV-Vis spectra, (D) IR spectre (E) Evolution of the FTIR spectra of the grafted silica with **SPI-4** as a function of temperature under vacuum (P= 10^{-6}) and (F) evolution of the intensity of the vibration band at 1390 cm^{-1} attributed to the C-H bending: (ref) pure silica, (1) grafted silica with **SPI-1** and (2) **SPI-4**. Ref correspond to the pure silica before grafting.

After determining the exact loading of grafted silica with SPI, the samples are subjected to Diffuse reflectance UV-visible and FTIR spectroscopies for further characterization. The new bands in DR UV-visible spectra (**Fi∈e 5(C)**) of **SPI -1** and **-4** positioned at 315, 276, 254 nm, and 240, 295 nm respectively, are characteristic of the benzoyl function and assigned to the electronic transitions $n-\pi^*$ (295-315 nm) and $\pi-\pi^*$(230-300 nm) of SPI molecules. Moreover, the additional intense band situated at 350 nm in the **SPI-4** spectrum corresponds to the $n-\pi^*$ electronic transitions of the nitrogen heteroatom in **SPI-4** structure. The presence of these characteristic bands, compared

to the UV-Visible spectra of the molecular **SPI -1** and **-4**, confirm that the grafting mechanism did not affect the chromophore part of the SPI structures. Additionally, by comparing the FTIR spectra (**Figure 5 (D)**) of the silica nanoparticles before and after grafting, new characteristic bands attributed to the grafted molecules are observed and are summarized and attributed in **Table S4** in the SI. The disappearance of the isolated silanol groups at 3744 cm^{-1} after grafting of **SPI-4** (**Figure S29)** confirms that the grafting mechanism is similar to that previously reported.[24, 26]

In contrast to the solvent-based chemical grafting, which has several significant technological and environmental disadvantages[35], dry surface functionalization is considered more environmentally friendly, since it is occurs in the absence of a solvent[36]. The TGA and FTIR spectra illustrating the difference in modified nanosilica, prepared by the two different grafting methods are reported in **Figure S30** and **Figure S31** in the supplementary information. The results reveal uniform distribution and similar loading of silane with both methods indicating the unnecessary excessive use of solvent for grafting the SPI compounds. The thermal stability of silica_**SPI-4** is investigated using in-situ FTIR under vacuum conditions (10^{-5} torr). The evolution of the IR spectra of silica_**SPI-4** is reported in **Figure 5(E)** and the evolution of the vibration band at 1390 cm^{-1} characteristic of grafted **SPI -1** and -**4** at different temperatures is reported in **Figure 5(F).** The results show a low amount of physisorbed species (decrease from 125-225 °C ~ 8 % from the overall SPI amount) with a relatively high thermal stability (until 225 °C) of the residual species for both structures. These results agree with the results obtained from the TG analysis and demonstrate that the chemically grafted SPI is ranging between 92 and 95% of the total SPI content in silica_**SPI -1** and **-4**, respectively. Thus, the mechanism of grafting can be determined by the covalent bonds between the alkoxy groups of SPI and isolated silanol groups of the silica occurs via the formation of new Si-O-Si bonds and the release of alcohol molecules.

2.5 Preparation of silica@polymer hybrid materials using SPI -1 and -4

Moreover, the viscosity of the UV curable dispersion is a key parameter which needs to be considered in order to control UV-curing kinetics as well as the processability of the system. It typically reveals particle-particle and particle-monomer interactions. The viscosities (measured at shear rate of 100 s^{-1}) as a function of grafted nanosilica content in TMPTA monomer mixtures are represented in **Figure 6**. As could be expected, the viscosity of the TMPTA filled with grafted silica nanoparticles displays the lowest value compared to that with ungrafted silica and increases with the increase of the filler content. This is due to the agglomeration of ungrafted nanoparticles yielding highly viscous dispersion due to the presence of silanol groups on the silica surface (**Figure 5(D)**). On the contrary, the modified silica nanoparticles have shown an improved compatibility with TMPTA, due to the formation of the organic shell of SPI and the decrease of the silanol content on the nanosilica surface. This leads to the enhancement of the hydrophobic/hydrophilic interactions of the dispersion medium and the dispersion phase. The viscosities of the formulations containing modified nanosized silica (grafted with equimolar amount of **SPI -1** and **-4**) reveal some differences at shear rate of 100 s^{-1} which could be assigned to a higher polarity of the **SPI-4**. As a consequence, 25 wt. % of silica_**SPI -1** and **-4** dispersed in TMPTA was chosen as appropriate filler loading. At this loading, photoinitiator content can sufficiently initiate photopolymerization process, while maintaining an appropriate viscosity for stereolithography applications (up to 10 Pa.s for 100 s^{-1} in 26 °C [37]).

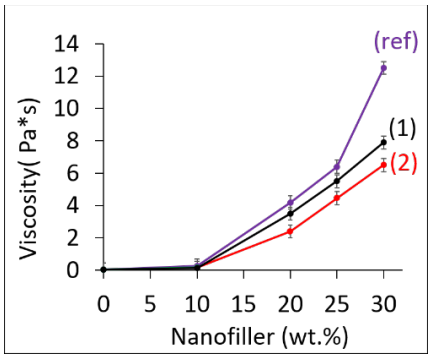

Figure 6. Evolution of the viscosity of the TMPTA with the amounts of the fillers: (ref) pure (non-grafted) silica, (1) grafted silica with **SPI -1** and (2) **SPI-4.**

The photopolymerization kinetics of the previously determined formula (25 wt. % of silica_**SPI-1/TMPTA** and silica_**SPI-4/TMPA**) are reported in **Figure 7** under various irradiation conditions. The comparison of the conversion yields of the different filler concentration formulations are presented in **Figure S32**. The shape of the conversion curves for silica_**SPI-4/TMPTA** under irradiation at 365 nm and 385 nm is characteristic of a photopolymerization with direct initiation, accompanied by the maximum polymerization rate and incomplete conversion of double bonds (**Figure 7(A)** and **(B)**). Additionally, an induction time is observed for silica_**SPI-1/TMPTA** and silica_**SPI-4/TMPA** samples under irradiation at 365 nm and 405 nm, respectively (**Figure 7 (A)** and **(C)**). Accordingly, the kinetics of polymerization decrease after grafting SPI on the surface of silica nanoparticles. This might be due to the presence of the silica particles that hinders the movements of the polymer chains and/or causing a shading effect. At the same time no significant difference between the final conversion yields is revealed according to SPI/TMPTA photopolymerization results. Thus, silica_**SPI-4** shows a high conversion yield (45 %) under irradiation at 365 nm with a decrease to 39 % at 385 nm and to 33 % at 405 nm. However, silica_**SPI-1** shows low activity under 365 nm irradiation with a conversion yield of 30 %, in

agreement with the activity of the pure **SPI-1** structure (**Figure 2**). These results indicate that the activity of the new **SPI-4** structure is not altered by the grafting process which is very promising for preparing hybrid materials under soft irradiation conditions. We should mention that the choice of the TMPTA as monomer is due to its desirable viscosity for both photopolymerization (homogeneous and hybrid). However, **SPI -1** and -**4** were also tested in the photopolymerization of the di-ethylene glycol di-acrylate (DEGDA, bifunctional acrylate) and methacrylate (MA, monofunctional acrylate) monomers. The results are assembled in **Figure S33** and **Figure S34**, respectively, and demonstrate that **SPI-4** presents always higher activity than **SPI-1** under various irradiation conditions for polymerizing acrylate-based monomers (mono-, bi- and tri-acrylate). It should be noted that the induction time observed in the case of MA is probably assigned to a higher quenching of the SPI triplet state by the monomer and/or dissolved oxygen (more significant at lower viscosity).

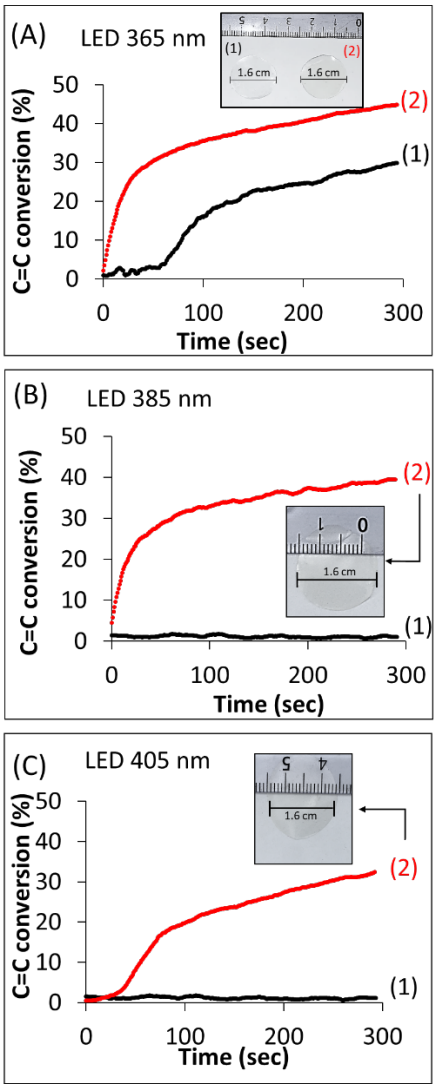

Figure 7. Photopolymerization, in lamellar (air-free) condition, of trimethylolpropane triacrylate (TMPTA) under 365 nm (A), 385 nm (B) and 405 nm (C) of irradiation using 25 wt. % of silica_**SPI-1** (1) and silica_**SPI-4** (2). Images in insert correspond to the corresponding photocured films obtained after the photopolymerization under the given conditions.

To test the possible spatial resolution of the photopolymerization once silica_**SPI-4** is used as photoactive filler, a homemade printed mask has been used to limit the light transmittance (405 nm) to the desired zone. The images of the corresponding films are reported in **Figure 8**. After

washing the polymerized film, the none photopolymerized part was easily removed via a sample wash with ethanol (**Figure 8**) demonstrating that the photopolymerization occurred selectively in the irradiated zones and that the hybrid silica-polymer can be spatially controlled as in the case of a conventional photopolymerizable systems. The SEM images demonstrate an interesting spatial resolution and the EDX mapping shows a homogeneous dispersion and embedded of the silica filler in the polymer matrix. It should be noted that the deterioration of some the letters is happing during their transfer from the polymer support to the SEM-support.

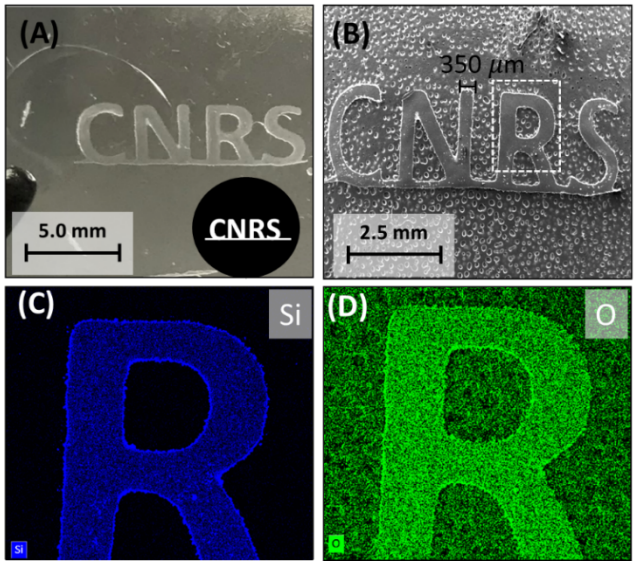

Figure 8. (A) Optical and (B) SEM images of the polymer-silica films after photopolymerization of TMPTA in presence of 25 wt.% of grated silica with **SPI-4** under 405 nm of irradiation for 2 min, using an ink-jet printed mask. The logo in insert of the picture (A) corresponds to that used for printing the masks on plastic papers using an ordinary ink-jet printer where the white color indicates the positive zones. (C) & (D) EDX mapping of the selected zone in (B) with "Si" and "O", respectively.

Finally, the mechanical properties of the composites' films prepared using SPI-4/silica were performed using atomic force microscopy (AFM)[38, 39]. Three films with a thickness around 50 μm were prepared under 385 nm for 5 min from three photopolymerizable formula: TMPTA+P-SPI-4 (pure polymer), TMPTA + P-SPI-4 + ungrafted silica and TMPTA+Silica-SPI-4. The results are assembled in **Figure 9** and show the AFM topographic and mechanical maps obtained for pure photopolymer film, and of the composites' films prepared in presence of ungrafted silica and by using silica-SPI-4. Smooth surfaces with roughness lower than 1 nm were demonstrated by the topographies of the surface of all films. Interestingly, the composite film prepared with SPI-4/silica nanoparticles shows nanodomains (≈50 nm) having high elastic modulus, associated to the silica nanoparticles. For the film prepared in presence of ungrafted silica (using P-SPI-4 as photoinitiator), aggregations of silica nanoparticles are most likely localized into the bulk of the film. These results are in agreement with our previous work obtained with SPI-1.[24] They demonstrate an enhancement of the mechanical properties of the composites once silica-SPI are used as photoinitiator fillers. The elastic modulus of the silica-SPI/Polymer composites is found to be 2 to 3 times higher compared to the pure polymer, or composite prepared with ungrafted silica. This increase is mainly assigned to the high dispersion and homogeneous silica nanoparticles and their chemical connection with the polymer matrices.

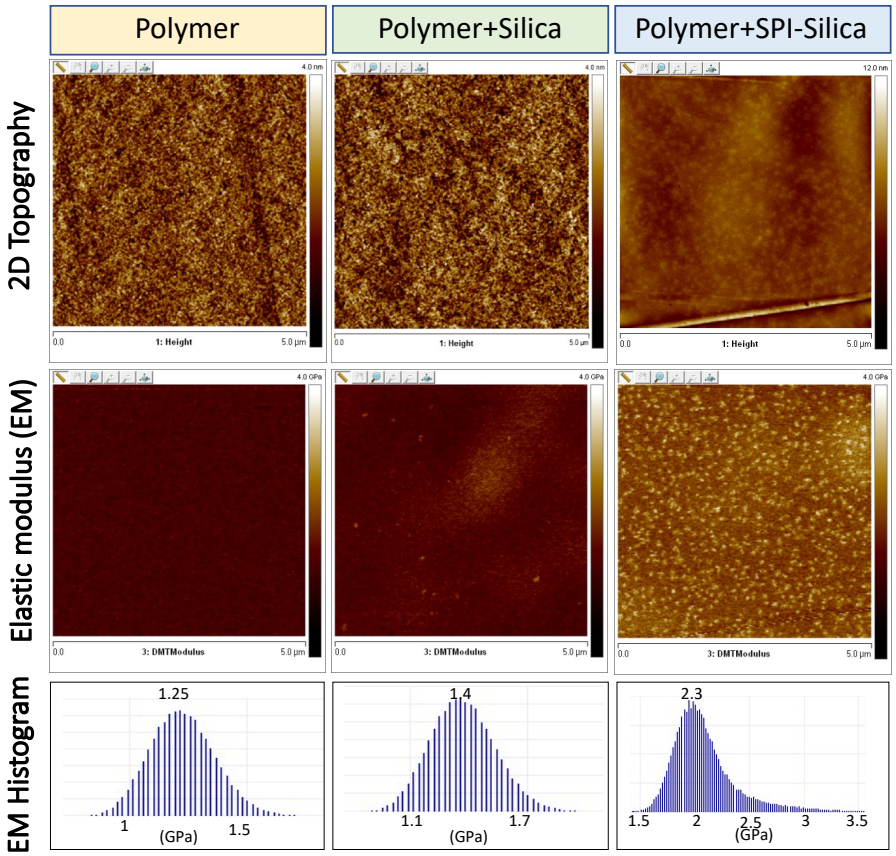

Figure 9. The AFM 2D-topographic images (top) at 5x5 μm scale, the elastic modulus (EM) mechanical maps (middle, z scale 4 GPa) and the corresponding histograms (bottom) of pure polymer (left), composite prepared with ungrafted silica (middle) and with silica-SPI-4 fillers (right). The light areas in the elastic modulus correspond to a higher rigidity of the analyzed zone and the white dotes nanodomain (≈50 nm) observed in the EM for the silica-SPI-4-Polymer film assigned to the highly dispersed silica nanoparticles near to the surface. Z-scale of the EM is identical for all images.

3. CONCLUSION

Five new bifunctional coupling agent structures have been synthesized form three steps synthesis pathway using recyclable heterogeneous Pt/Al_2O_3 catalyst and tested for preparing filler-polymer hybrid materials. The triphenylamine based structures (**SPI-4** to **6**) showed the highest activity under the various irradiation conditions going from UV-B to the visible light. Particularly, the cost-effective **SPI-4** structure can be easily scaled up and therefore it is considered as promising candidate for preparing hybrid material by photopolymerization under soft irradiation condition. The activity of the **SPI-4** was tested in the photopolymerization of mono- (MA) bi- (DEGDA) and tri- (TMPTA) functional acrylate-based monomers and compared to that obtained with SPI-1. A higher activity of SPI-4 under the various irradiation conditions (365nm, 385 nm, and 405 nm) was obtained and mainly assigned to its high absorbance of light (higher quantum yield) with similar activity of the grafted radical moiety in respect to SPI-1. The spatial and temporal control of the process as well as the enhancement of the elastic modulus of the composite are demonstrated and assigned to a higher dispersion of the filler in the polymer matrices as well as to the formation of covalent chemical bonds between the nanoparticles as fillers and the polymer. This work opens the way for preparing new materials for various applications such as membrane, 3D-printing, medicine, photo- and stereo- lithography using various acrylate-based polymer or filler materials (e.g. zeolite, TiO_2, etc.).

Supporting information

The following data and information are available free of charge via the Internet: list of materials used in this work; experimental part including the methods for characterization; detailed synthesis procedures and conditions; NMR spectra of the organic compounds; grafting procedure

of the **SPI-X** on the silica and the photopolymerization procedure; photopolymerization kinetic of **P-1-SPI-4** and **SPI-4**; table summarizing the polymerization rates; the lifetime of the triplet excited states; characteristic vibrational bands; comparison between the two grafting methods; and the conversion yields at different silica_**SPI-4** loadings and photopolymerization kinetics of di-ethylene glycol di-acrylate and methacrylate using SPI-4 and SPI-1 .

AUTHOR INFORMATION

Corresponding Author

* Mohamad El-Roz: mohamad.elroz@ensicaen.fr

Present Addresses

[a]Normandie Université, ENSICAEN, UNICAEN, CNRS, Laboratoire Catalyse et Spectrochimie, 14050 Caen, France.

[b]Normandie Université, ENSICAEN, UNICAEN, CNRS, Laboratoire CRISMAT, 14050 Caen, France.

[c] Université de Toulon, Laboratoire MAPIEM, 83041 Toulon, France

Author Contributions

The manuscript was written through contributions of all authors. All authors have given approval to the final version of the manuscript. ‡These authors contributed equally: Houssein Nasrallah, Rita Zakhia Douaihy.

ACKNOWLEDGMENT

Authors acknowledge the European Union and the Carnot EPS institute for the financial support (3DZeoPol project). Authors acknowledge Dr. Jaafar El Fallah for helping in the SEM analysis.

REFERENCES

1. Wang, M.; Hao, X.; Wang, W., Reinforcing Behaviors of Sulfur-Containing Silane Coupling Agent in Natural Rubber-Based Magnetorheological Elastomers with Various Vulcanization Systems. *Materials* **2020,** *13* (22), 5163.
2. Pan, C.; Kou, K.; Jia, Q.; Zhang, Y.; Wu, G.; Ji, T., Improved thermal conductivity and dielectric properties of hBN/PTFE composites via surface treatment by silane coupling agent. *Composites Part B: Engineering* **2017,** *111*, 83-90.
3. Wu, G.; Cheng, Y.; Wang, Z.; Wang, K.; Feng, A., In situ polymerization of modified graphene/polyimide composite with improved mechanical and thermal properties. *Journal of Materials Science: Materials in Electronics* **2017,** *28* (1), 576-581.
4. Attharangsan, S.; Saikrasun, S., Corn cob powder (CCP) Filled Natural Rubber (NR) composites with Si69 as coupling agent: effect of Si69 content on properties of the composites. *International Journal of Science and Innovative Technology* **2021,** *4* (1), 59-69.
5. Zheng, J.; Han, D.; Ye, X.; Wu, X.; Wu, Y.; Wang, Y.; Zhang, L., Chemical and physical interaction between silane coupling agent with long arms and silica and its effect on silica/natural rubber composites. *Polymer* **2018,** *135*, 200-210.
6. Kahraman, M. V.; Kayaman-Apohan, N.; Akdemir, Z. S.; Boztoprak, Y.; Güngör, A., Synthesis of a novel bifunctional photoinitiator: hybrid coatings on polycarbonate. *Macromolecular Chemistry and Physics* **2007,** *208* (14), 1572-1581.
7. Buestrich, R.; Kahlenberg, F.; Popall, M.; Dannberg, P.; Müller-Fiedler, R.; Rösch, O., ORMOCER® s for optical interconnection technology. *Journal of Sol-Gel Science and Technology* **2001,** *20* (2), 181-186.
8. Kahraman, M. V.; Kuğu, M.; Menceloğlu, Y.; Kayaman-Apohan, N.; Güngör, A., The novel use of organo alkoxy silane for the synthesis of organic–inorganic hybrid coatings. *Journal of non-crystalline solids* **2006,** *352* (21-22), 2143-2151.
9. Dietlin, C.; Schweizer, S.; Xiao, P.; Zhang, J.; Morlet-Savary, F.; Graff, B.; Fouassier, J.-P.; Lalevée, J., Photopolymerization upon LEDs: New photoinitiating systems and strategies. *Polymer Chemistry* **2015,** *6* (21), 3895-3912.
10. Zhang, Y.; Xu, Y.; Simon-Masseron, A.; Lalevée, J., Radical photoinitiation with LEDs and applications in the 3D printing of composites. *Chemical Society Reviews* **2021,** *50* (6), 3824-3841.
11. Layani, M.; Wang, X.; Magdassi, S., Novel materials for 3D printing by photopolymerization. *Advanced Materials* **2018,** *30* (41), 1706344.
12. Zhao, L.; Zhang, M.; Chitrakar, B.; Adhikari, B., Recent advances in functional 3D printing of foods: A review of functions of ingredients and internal structures. *Critical Reviews in Food Science and Nutrition* **2021,** *61* (21), 3489-3503.
13. Mendes-Felipe, C.; Oliveira, J.; Etxebarria, I.; Vilas-Vilela, J. L.; Lanceros-Mendez, S., State-of-the-art and future challenges of UV curable polymer-based smart materials for printing technologies. *Advanced Materials Technologies* **2019,** *4* (3), 1800618.

14. Zheng, Z.; Eglin, D.; Alini, M.; Richards, G. R.; Qin, L.; Lai, Y., Visible light-induced 3D bioprinting technologies and corresponding bioink materials for tissue engineering: A review. *Engineering* **2021,** *7* (7), 966-978.
15. Xu, X.; Awad, A.; Robles-Martinez, P.; Gaisford, S.; Goyanes, A.; Basit, A. W., Vat photopolymerization 3D printing for advanced drug delivery and medical device applications. *Journal of Controlled Release* **2021,** *329*, 743-757.
16. Kessler, A.; Hickel, R.; Reymus, M., 3D printing in dentistry—state of the art. *Operative dentistry* **2020,** *45* (1), 30-40.
17. Elshereksi, N. W.; Ghazali, M.; Muchtar, A.; Azhari, C. H., Review of titanate coupling agents and their application for dental composite fabrication. *Dental materials journal* **2017**, 2016-014.
18. Wang, H.; He, Y.; Fei, G.; Wang, C.; Shen, Y.; Zhu, K.; Sun, L.; Rang, N.; Guo, D.; Wallace, G. G., Functionalizing graphene with titanate coupling agents as reinforcement for one-component waterborne poly (urethane-acrylate) anticorrosion coatings. *Chemical Engineering Journal* **2019,** *359*, 331-343.
19. Ahangaran, F.; Navarchian, A. H., Recent advances in chemical surface modification of metal oxide nanoparticles with silane coupling agents: A review. *Advances in Colloid and Interface Science* **2020,** *286*, 102298.
20. Shokoohi, S.; Arefazar, A.; Khosrokhavar, R., Silane coupling agents in polymer-based reinforced composites: a review. *Journal of Reinforced Plastics and Composites* **2008,** *27* (5), 473-485.
21. Provost, M.; Raulin, K.; Maindron, T.; Gaud, V., Influence of silane coupling agent on the properties of UV curable SiO2-PMMA hybrid nanocomposite. *Journal of Sol-Gel Science and Technology* **2019,** *89* (3), 796-806.
22. Liu, F.; Liu, A.; Tao, W.; Yang, Y., Preparation of UV curable organic/inorganic hybrid coatings-a review. *Progress in Organic Coatings* **2020,** *145*, 105685.
23. EL ROZ, M. L., Sami ; TELEGEIEV, Igor New photoinitiator based on bifunctional silane. *CNRS innovation* **2017**.
24. Douaihy, R. Z.; Telegeiev, I.; Nasrallah, H.; Lebedev, O.; Bazin, P.; Vimont, A.; Chailan, J.-F.; Fahs, A.; Mohamad, E.-R., Synthesis of silica-polymer core-shell hybrid materials with enhanced mechanical properties using a new bifunctional silane-based photoinitiator as coupling agent. *Materials Today Communications* **2021**, 102248.
25. Blume, A.; El-Roz, M.; Thibault-Starzyk, F., Infrared study of the silica/silane reaction. *11 Kautschuk Herbst Kolloqium* **2014**.
26. El-Roz, M.; Thibault-Starzyk, F.; Blume, A., Infrared study of the silica/silane reaction. Part II. *KGK Kautschuk, Gummi, Kunststoffe* **2014,** *67* (5), 53-57.
27. Yoshino, F.; Yoshida, A., Effects of blue-light irradiation during dental treatment. *Japanese Dental Science Review* **2018,** *54* (4), 160-168.
28. Ibrahim-Ouali, M.; Dumur, F., Recent advances on chalcone-based photoinitiators of polymerization. *European Polymer Journal* **2021,** *158*, 110688.
29. Peng, X.; Zhang, J.; Stachurski, Z. H.; Banaszak Holl, M. M.; Xiao, P., Visible-Light-Sensitive Triazine-Coated Silica Nanoparticles: A Dual Role Approach to Polymer Nanocomposite Materials with Enhanced Properties. *ACS Applied Materials & Interfaces* **2021,** *13* (38), 46033-46042.

30. Xie, X.; Zhang, X.; Yang, H.; Ji, X.; Li, J.; Ding, S., Iridium-catalyzed hydrosilylation of unactivated alkenes: scope and application to late-stage functionalization. *The Journal of Organic Chemistry* **2018,** *84* (2), 1085-1093.
31. Glaser, P. B.; Tilley, T. D., Catalytic hydrosilylation of alkenes by a ruthenium silylene complex. Evidence for a new hydrosilylation mechanism. *Journal of the American Chemical Society* **2003,** *125* (45), 13640-13641.
32. Li, S. L.; Xu, X.; Truhlar, D. G., Computational simulation and interpretation of the low-lying excited electronic states and electronic spectrum of thioanisole. *Physical Chemistry Chemical Physics* **2015,** *17* (31), 20093-20099.
33. Gališinová, J.; Andriamainty, F.; Malík, I.; Čižmárik, J.; Karlovska, J.; Sichrovska, L., A Study of Local Anaesthetics. Part 202. Determination of the Critical Micellar Concentration of Carbisocainium Chloride in Water Using Spectral Methods and the Probe Pyrene. *European Pharmaceutical Journal* **2013,** *60* (1), 1-6.
34. Hou, X.-Y.; Li, T. C.; Yin, C.-R.; Xu, H.; Lin, J.; Hua, Y.-R.; Chen, D.-Y.; Xie, L.-H.; Huang, W., Stable hole-transporting molecular glasses based on complicated 9, 9-diarylfluorenes (CDAFs). *Synthetic metals* **2009,** *159* (11), 1055-1060.
35. Telegeev, I.; Voronin, E.; Pakhlov, E.; Kalibabchuk, V., Modification of Nanosilica Surfaces by Methyl Methacrylate Oligomers. In *Nanoscience Advances in CBRN Agents Detection, Information and Energy Security*, Springer: 2015; pp 185-191.
36. He, X.; Mahtabani, A.; Rytöluoto, I.; Saarimäki, E.; Lahti, K.; Paajanen, M.; Anyszka, R.; Dierkes, W.; Blume, A. In *Surface modification of fumed silica by dry silanization for PP-based dielectric nanocomposites*, 2019 2nd International Conference on Electrical Materials and Power Equipment (ICEMPE), IEEE: 2019; pp 254-259.
37. Bertsch, A.; Jiguet, S.; Renaud, P., Microfabrication of ceramic components by microstereolithography. *Journal of micromechanics and microengineering* **2003,** *14* (2), 197.
38. BV, D.; VM, M.; YP, T., Effect of contact deformations on the adhesion of particles. *Journal of Colloid and Interface Science* **1975,** *53*, 314-326.
39. Muller, V.; Derjaguin, B.; Toporov, Y. P., On two methods of calculation of the force of sticking of an elastic sphere to a rigid plane. *Colloids and Surfaces* **1983,** *7* (3), 251-259.

For Table of Contents Only